ADVANCES IN ATMOSPHERIC SCIENCES, VOL. 32, MARCH 2015, 287–300

Assessment of the Biospheric Contribution to Surface Atmospheric CO_2 Concentrations over East Asia with a Regional Chemical Transport Model

KOU Xingxia[1,2], ZHANG Meigen[*1], PENG Zhen[3], and WANG Yinghong[1]

[1]*State Key Laboratory of Atmospheric Boundary Layer Physics and Atmospheric Chemistry, Institute of Atmospheric Physics, Chinese Academy of Sciences, Beijing* 100029

[2]*University of Chinese Academy of Sciences, Beijing* 100049

[3]*School of Atmospheric Sciences, Nanjing University, Nanjing* 210093

(Received 28 March 2014; revised 2 June 2014; accepted 25 June 2014)

ABSTRACT

A regional chemical transport model, RAMS-CMAQ, was employed to assess the impacts of biosphere–atmosphere CO_2 exchange on seasonal variations in atmospheric CO_2 concentrations over East Asia. Simulated CO_2 concentrations were compared with observations at 12 surface stations and the comparison showed they were generally in good agreement. Both observations and simulations suggested that surface CO_2 over East Asia features a summertime trough due to biospheric absorption, while in some urban areas surface CO_2 has a distinct summer peak, which could be attributed to the strong impact from anthropogenic emissions. Analysis of the model results indicated that biospheric fluxes and fossil-fuel emissions are comparably important in shaping spatial distributions of CO_2 near the surface over East Asia. Biospheric flux plays an important role in the prevailing spatial pattern of CO_2 enhancement and reduction on the synoptic scale due to the strong seasonality of biospheric CO_2 flux. The elevation of CO_2 levels by the biosphere during winter was found to be larger than 5 ppm in North China and Southeast China, and during summertime a significant depletion ($\geqslant$ 7 ppm) occurred in most areas, except for the Indo-China Peninsula where positive bioflux values were found.

Key words: CO_2 regional transport modeling, seasonal variation, biospheric flux

Citation: Kou, X. X, M. G. Zhang, Z. Peng, and Y. H. Wang, 2015: Assessment of the biospheric contribution to surface atmospheric CO_2 concentrations over East Asia with a regional chemical transport model. *Adv. Atmos. Sci.*, **32**(3), 287–300, doi: 10.1007/s00376-014-4059-6.

1. Introduction

Carbon dioxide (CO_2) is one of the most important greenhouse gases warming our atmosphere. Its temporal and spatial variability in the atmosphere reflects the influence of anthropogenic inputs, including fossil-fuel emissions, cement production, land-use change (mainly deforestation) and other human activities, as well as the removal by two known reservoirs: the ocean and the terrestrial biosphere (Morimoto et al., 2000; Liu et al., 2005; Piao et al., 2009). The remainder that stays in the atmosphere exhibits large diurnal, synoptic, seasonal and interannual variability, especially over land. Previous studies have found that most CO_2 emissions originate from cities due to human activities, even though urban areas cover only a small fraction of Earth's land area (Wang et al., 2012; Schneising et al., 2013). From the perspective of the natural carbon cycle, global terrestrial ecosystems absorb carbon at a rate of 1–4 Pg yr^{-1}, offsetting 10%–60% of fossil-fuel emissions, while the regional patterns of terrestrial carbon sources and sinks remain uncertain (Solomon et al., 2007; Zhao et al., 2012; Zhang et al., 2013). With increasing scientific and political interest in regional aspects of the global carbon cycle, there is a strong impetus to resolve fine-scale CO_2 transport and variability.

Atmospheric CO_2 is a particularly important climatic issue in East Asia because this area has experienced extensive industrialization in the last three decades with accumulated impacts of anthropogenic emissions and regionally distinct changes of land-use conditions and climate trends (Streets et al., 2003a; Zhang et al., 2009; Liu et al., 2013a; Wang et al., 2013). Previous efforts have shown some promising achievements with high-resolution regional chemical transport models (CTMs) (Chevillard et al., 2002; Sarrat et al., 2007; Ahmadov et al., 2009; Ballav et al., 2012). For example, Ahmadov et al. (2009) coupled the atmospheric Weather Research and Forecasting (WRF) model with a diagnostic biospheric model (Vegetation Photosynthesis and Respira-

* Corresponding author: ZHANG Meigen
Email: mgzhang@mail.iap.ac.cn

tion Model; VPRM) to understand the effects that mesoscale transport has on atmospheric CO_2 distributions. Also, WRF-Chem has been used for regional transport simulations with prescribed terrestrial biogenic flux input from two biogeochemical model simulations [Carnegie–Ames–Stanford Approach (CASA) and Simple Biosphere Model (SIB3)], and the results indicated that surface flux horizontal distributions and wind directions are the dominant controls for CO_2 synoptic variations (Ballav et al., 2012). Some key requirements for regional CO_2 modeling have been noted, such as using realistic initial and lateral boundary conditions, while issues that are of interest for the magnitude and spatial extent of biospheric and anthropogenic roles in atmospheric CO_2 have not yet been addressed in most regional modeling studies. Considering the unique characteristics (e.g., long atmospheric lifetime, large background concentration, and strong biosphere–atmosphere exchanges) of atmospheric CO_2 that are distinctly different from other traditionally modeled chemical pollutants, further study is therefore needed to gain insight into the biospheric and anthropogenic contributions to shaping the CO_2 spatial distribution and seasonal variations in East Asia.

By incorporating a VPRM in the online mode, the comprehensive regional air quality modeling system, RAMS-CMAQ (Regional Atmospheric Modeling System and Models-3 Community Multi-scale Air Quality) was developed to simulate atmospheric CO_2 concentrations over East Asia, and its feasibility in regional CO_2 modeling was demonstrated (Kou et al., 2013). The CO_2 volume fraction is transported as a tracer in this model, with prescribed surface CO_2 fluxes that include fossil-fuel emissions, biomass burning, air–sea CO_2 exchange, and biosphere–atmosphere CO_2 exchange. Biospheric flux is the net flux between uptake from photosynthesis and release from ecosystem respiration, and has been found to have significant impacts on surface CO_2 concentrations (Ahmadov et al., 2007; Piao et al., 2007; Le Quere et al., 2009; Peters et al., 2010; Liu et al., 2013b). Considering the high level of uncertainty in simulated bioflux in current terrestrial biosphere models (Canadell et al., 2007; Schaefer et al., 2012; Huntzinger et al., 2012, 2013), the widely recognized results from the CarbonTracker-2011 optimized estimation (CT2011_oi) were adopted in this study (Peters et al., 2007). The primary purpose of this study is to further investigate and understand the spatial distributions and seasonal variations of atmospheric CO_2 concentrations in East Asia on fine spatial scales; and then to identify and quantify the biospheric contribution with this modeling system. A description of the model and input data is given in section 2, followed by a presentation and discussion of the results in section 3. A summary and conclusions are provided in section 4.

2. Model description

The RAMS-CMAQ modeling system was developed based on the US Environmental Protection Agency's CMAQ, with RAMS providing the three-dimensional meteorological fields (Zhang et al., 2002), and was extended to include CO_2 simulation by Kou et al. (2013). The study domain for CMAQ was 6654×5440 km^2, with a grid resolution of 64×64 km^2 on a rotated polar stereographic map projection centered at (35.0°N, 116.0°E), and covered the whole area of East Asia (as shown in Fig. 1). The model system has 15 vertical layers in the σ_z-coordinate system, unequally spaced from the ground to approximately 23 km, with nearly half of them concentrated in the lowest 2 km (vertical resolution of 100–200 m from the ground to approximately 1.5 km) to resolve the planetary boundary layer. The output time step is 1 h. CO_2 is treated in the model as an inert chemical species, whose concentrations are determined by atmospheric transport (horizontal and vertical advection and diffusion) and four types of prescribed fluxes.

The fossil-fuel emissions were adopted from the Regional Emission Inventory in Asia, with monthly gridded data at a $0.25^\circ \times 0.25^\circ$ resolution (REAS v2.1; Kurokawa et al., 2013). The REAS estimates the emissions from fuel combustion sources and non-combustion sources, including power, industry, transport, and other sectors (e.g., commercial and residential). Biomass-burning emissions from forest wildfires, savanna burning and slash-and-burn agriculture were provided by the Global Fire Emissions Database monthly mean inventory at a spatial resolution of $0.5^\circ \times 0.5^\circ$ (GFED v3; van der Werf et al., 2010). As mentioned above, biosphere–atmosphere exchange and ocean flux were obtained from CT2011_oi [global resolution of 3° (lon) $\times 2^\circ$ (lat), 3 hourly]. The National Oceanic and Atmospheric Administration's (NOAA) CarbonTracker, used in this study, is an example of a data assimilation system that provides optimized biosphere and ocean CO_2 fluxes using *in situ* CO_2 observations from a global observational network and prior biospheric flux from the CASA model (Peters et al., 2007).

Figure 2 shows the seasonal mean distribution of biospheric fluxes and ocean flux (Figs. 2a–d), and fossil-fuel and biomass-burning emissions (Figs. 2e–h) in the model domain. In Figs. 2a–d, negative values indicate the removal of CO_2 from the atmosphere to the biosphere, and positive values indicate the release of CO_2 to the atmosphere. The seasonal and spatial variation of biospheric CO_2 flux in East Asia is strongly influenced by the seasonal growth and decay of plants in terrestrial ecosystems, which is mainly driven by the seasonal variation of precipitation, temperature, photosynthetically active solar radiation, and other meteorological factors (Fu et al., 2009). Generally, the biosphere absorbs CO_2 in summer, as the uptake of atmospheric CO_2 by photosynthesis exceeds CO_2 released by respiration in the growing season. While in winter, the biosphere acts as a source since CO_2 released by respiration exceeds uptake by photosynthesis (Figs. 2a and 2c). It should be noted that South East Asia (the Indo-China Peninsula) displays distinctively different seasonal patterns of CO_2 exchange, with strong absorption in winter and release in summer, since photosynthesis is taking place under unfavorable conditions (i.e., the exces-

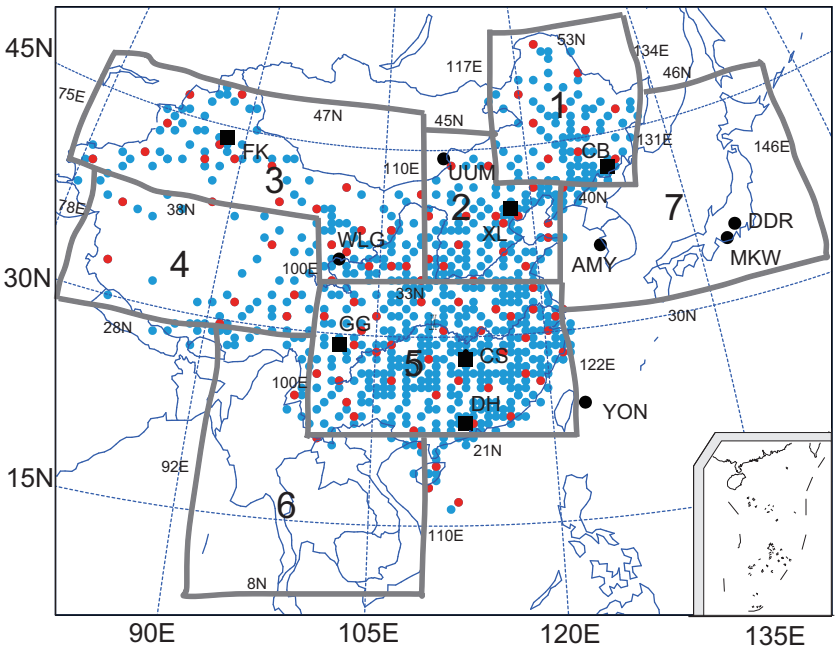

Fig. 1. Locations of observation stations: 838 meteorological stations (blue dots), among which 99 stations provided total solar radiation measurements (red dots) and 12 CO_2 monitoring sites (black dots—AMY, DDR, MKW, UUM, WLG and YON; black squares— CB, CS, DH, FK, GG, and XL). The seven sub-regions in the model domain, which partly follows the conventional division of geographical regions for comparing fluxes and concentrations, are also shown: 1 Northeast China; 2 North China; 3 Northwest China and South Mongolia; 4 Southwest China; 5 Southeast China; 6 South East Asia (Indo-China Peninsula); 7 Korea peninsula and Japan.

sive precipitation delivered by the southern Asian monsoon and insufficient photosynthetically active radiation during the rainy season), while respiration increases with the rising temperature (Yu et al., 2013).

Figures 2e–h show the seasonality of fossil-fuel and biomass-burning emissions in the model domain for 2010. Compared to bioflux, the horizontal distribution patterns of fossil-fuel emissions show considerable spatial heterogeneity and large gradients (Fig. 2e). They also display a lower degree of seasonality, but with a peak during wintertime (Figs. 2f–h and Table 1) in most areas due to increased energy consumption to meet the electricity demands for air conditioning and heating, especially in the north of China (Gurney et al., 2005; Wang et al., 2012; Zhao et al., 2012; Liu et al., 2013a). The increase in Southeast Asia (Fig. 2f) could be primarily attributable to the rise of biomass burning during springtime (Streets et al., 2003b). Biomass-burning emissions (Lü et al., 2006) and ocean–atmosphere CO_2 fluxes (Xu et al., 2013) also show seasonal variation, but are of minor importance compared to the biospheric and fossil-fuel fluxes in the model domain (Table 1 and Fig. 2). Fully understanding the effects of biomass burning and ocean flux is outside the scope

Table 1. Monthly mean CO_2 fluxes used in the CMAQ simulation over the model domain (units: Tg C month^{-1}).

Month	Fossil fuels	Biomass burning	Bioflux	Ocean flux	Total fluxes
January	338.34	19.69	67.50	−9.78	415.75
February	317.19	26.25	38.84	−12.28	370.00
March	325.09	141.57	60.40	−13.32	513.74
April	313.02	23.15	80.10	−15.88	400.39
May	306.39	2.58	84.48	−9.41	384.04
June	322.83	2.45	−391.66	−7.91	−74.29
July	314.56	0.79	−344.48	0.50	−28.63
August	311.17	0.89	−381.72	2.44	−67.22
September	315.78	1.45	−122.10	0.84	195.97
October	310.65	0.99	30.26	−4.68	337.22
November	344.97	0.29	95.89	−8.95	432.20
December	363.80	1.00	68.26	−22.72	410.34

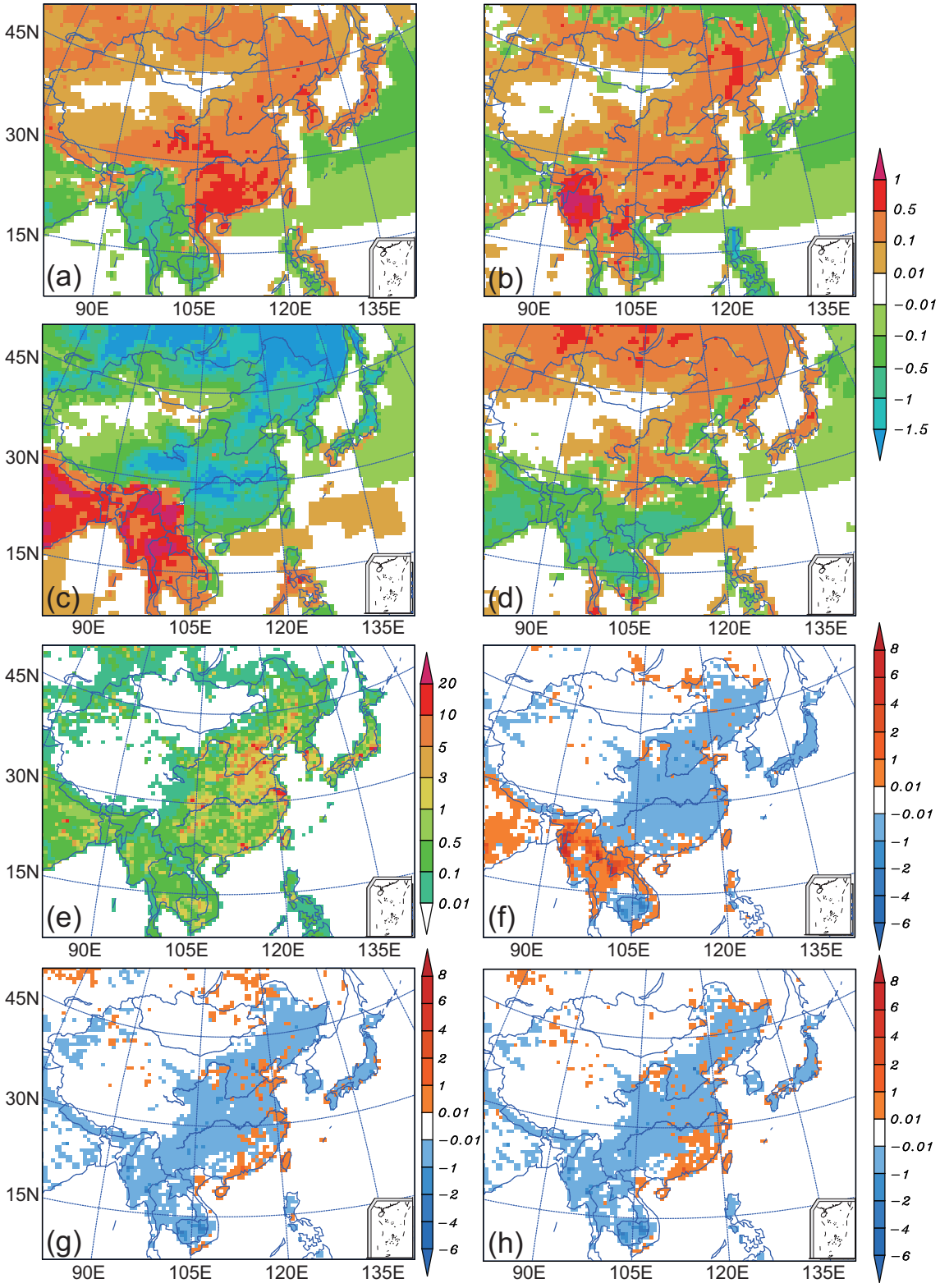

Fig. 2. Horizontal distribution of bioflux in (a) winter (December–February), (b) spring (March–May), (c) summer (June–August) and (d) autumn (September–November) (with ocean flux also given over ocean areas). Fossil-fuel and biomass-burning emissions in (e) winter, and the difference between (f) spring and winter, (g) summer and winter, and (h) autumn and winter of 2010 (units: μmol m^{-2} s^{-1}).

of this work and is not discussed further here.

The spatial pattern of CO_2 net flux (i.e., the sum of these four types of fluxes) shown in Fig. 3 retains features from both the bioflux and fossil-fuel emissions, which is attributable to their comparable flux magnitudes in the model domain (Fig. 2). During wintertime (Fig. 3a), the biosphere acts as a source, which further magnifies the CO_2 net flux on the basis of increased anthropogenic input; while during spring, summer, and autumn (Figs. 3b–d), some fossil-fuel emissions are offset by negative bioflux, thus resulting in a neutral (zero) or negative net flux in the biospheric sink functional areas (e.g., Northwest China and Inner Mongolia). The modeling system executed simultaneous simulations of CO_2 continuously from 26 December 2009 to 31 December 2010, starting at 0000 UTC 26 December. In this study, the initial fields and boundary conditions of atmospheric CO_2 volume fraction were obtained by interpolation of CT2011 optimized estimation (CT2011_oi; data available at http://carbontracker.noaa.gov). To understand the role of biospheric flux, atmospheric CO_2 was simulated by CMAQ using two set fluxes. The first was designed as the standard simulation with prescribed flux including fossil-fuel emissions, biomass-burning emissions, biospheric and ocean fluxes to investigate the CO_2 spatial distribution. The second was performed as the comparison simulation, which was similar to the former but without biospheric flux (i.e., only fossil-fuel emissions, biomass-burning emissions, and ocean flux included). The biospheric contribution to surface CO_2 concentration was obtained by subtracting the results of the comparison simulation from the standard one.

3. Results and discussion

3.1. *Model evaluation*

An evaluation of temperature, precipitation, wind speed, and total solar radiation is first presented in order to diagnose the strengths and weaknesses in the simulated meteorological conditions. The locations of observation stations are given in Fig. 1, and Fig. 4 shows a comparison between simulated and ground-based measurements. Observational surface temperature, precipitation and wind speed were obtained from 838 Chinese stations, among which 99 stations provided total solar radiation measurements. As shown in Fig. 4, the simulated and observed results were generally in good agreement (Figs. 4a–d). The summertime ridge of temperature, precipitation and total solar radiation was well captured by the model. Major deficiencies in the RAMS simulations included an underestimation of precipitation and an overestimation of total solar radiation. This could be attributable to the bias in simulation for the southern part of China, which is likely to be predominantly associated with the cloud–radiation transfer parameterization (Leung et al., 1999; Ge et al., 2011). Wind speed was well reproduced by the model in most months (Fig. 4c). The comparison led to confidence in the meteorological conditions provided by RAMS and verified that the configuration of the simulation adopted in this study was suitable for studying the transport of CO_2 with prescribed fluxes in East

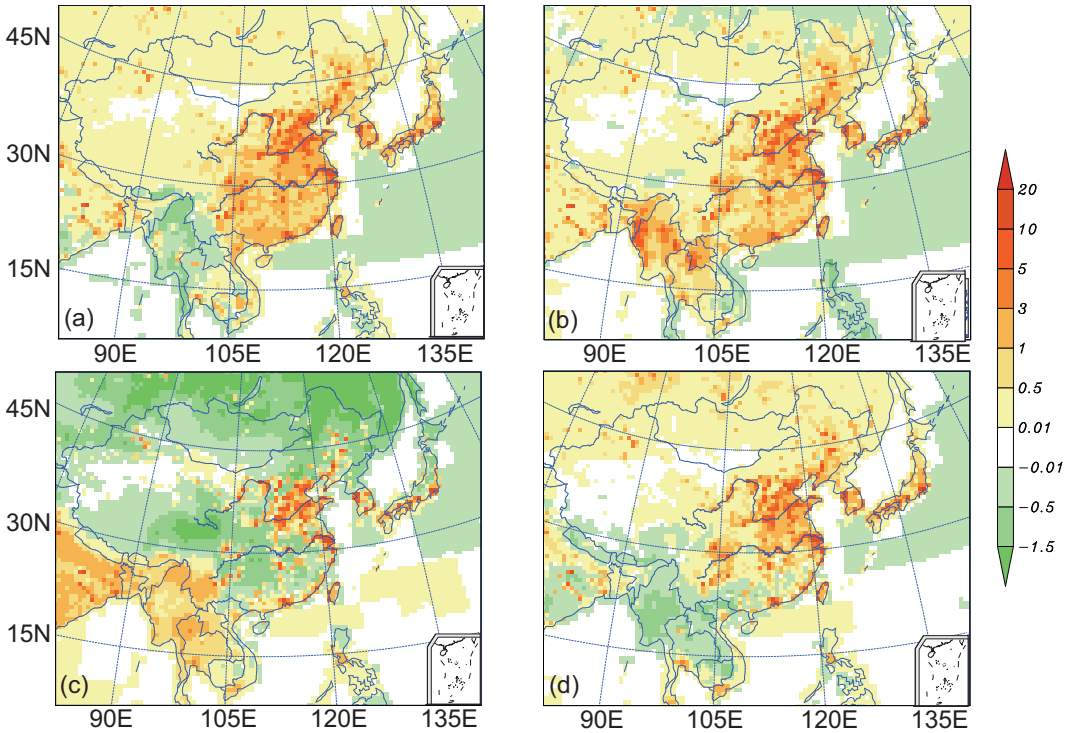

Fig. 3. The same as Fig. 2, but for CO_2 net fluxes (i.e., the sum of fossil-fuel emissions, biomass burning, ocean flux, and biosphere–atmosphere exchange): (a) winter, (b) spring, (c) summer, and (d) autumn (units: μmol m^{-2} s^{-1}).

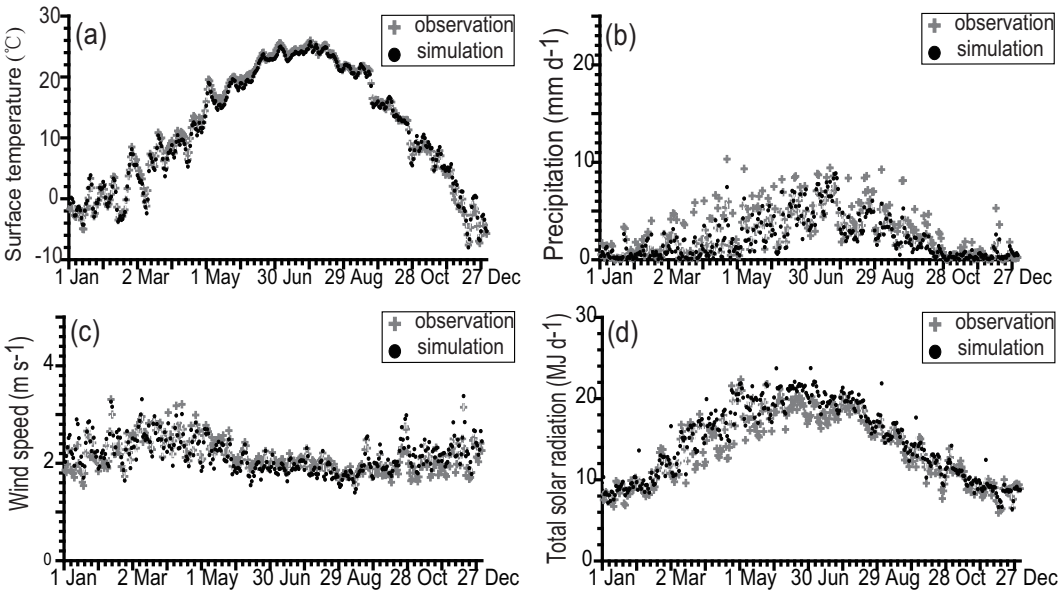

Fig. 4. Comparison of model results at the lowest model layer (∼50 m AGL) (black) and observations at ground level (grey): (a) averaged daily surface temperature (°C) of the 838 observation stations. Panel (b) is the same as (a) but for precipitation (mm d^{-1}), and (c) is the same as (a) but for wind speed (units: m s^{-1}). (d) Total solar radiation (MJ d^{-1}) of the 99 observation stations.

Asia.

The modeled CO_2 mixing ratios were then compared with ground-based in-situ measurements from the World Data Centre for Greenhouse Gases (WDCGG, http://ds.data.jma.go.jp/gmd/wdcgg/) and Chinese Ecosystem Research Network (CERN). The geographical information of 12 East Asian observation stations is listed in Table 2, which could be classified generally as coastal, remote ocean, mountain, and inland stations. Figures 5 and 6 show the observed and simulated monthly-averaged CO_2 concentrations at these stations from January to December of 2010. For the six WDCGG stations [AMY (Lee and Kim, 2013), DDR (Muto, 2013), MKW (Ohno, 2011), UUM (Conway, 2013), WLG (Zhou, 2013) and YON (Fukuyama, 2013)], the observed data at hourly time intervals were obtained. Thus, the monthly means of the simulation and observation were both calculated from the daily means based on hourly outputs, with the standard deviation of the simulation provided (Fig. 5). For the six CERN stations (Changbai Mountains, Changsha, Dinghu Mountains, Fukang, Gongga Mountains, and Xinglong), the observed monthly means were calculated from four weekly measurements (in cases of no missing data), and the weekly-mean values were created from instantaneous *in-situ* measurements every seven days. The simulated monthly CO_2 means used to compare with the CERN observations were calculated from daily means with the standard deviation provided (Fig. 6).

A comparison of the stations where land flux dominated is discussed in order to further evaluate CMAQ-simulated temporal variations (on a monthly basis) and analyze the underlying factors driving the observed seasonal variability of CO_2. Examples of monthly mean CO_2 concentrations from CMAQ and observations are shown in Fig. 5 for six stations (AMY, DDR, MKW, UUM, WLG and YON), and the statistical char-

Table 2. Location and general description of the observation sites.

Station	Latitude (°N)	Longitude (°E)	Altitude (m)	Country	General site description
1 AMY (Anmyeon-do)	36.53	126.32	47.0	Korea	Coastal
2 DDR (Mt. Dodaira)	36.00	139.18	840.0	Japan	Mountain
3 MKW (Mikawa-Ichinomiya)	34.85	137.43	50.0	Japan	Inland (urban)
4 UUM (Ulaan Uul)	44.45	111.08	914.0	Mongolia	Inland (grassland)
5 WLG (Mt. Waliguan)	36.30	100.90	3810.0	China	Inland (plateau)
6 YON (Yonagunijima)	24.47	123.02	30.0	Japan	Remote Ocean
7 Changbai Mt. (CB)	42.40	128.01	738.0	China	Mountain (temperate forest)
8 Changsha (CS)	28.21	113.06	44.0	China	Inland (urban)
9 Dinghu Mt. (DH)	23.17	112.50	90.0	China	Mountain (subtropical forest)
10 Fukang (FK)	44.28	87.92	460.0	China	Inland (desert)
11 Gongga Mt. (GG)	29.51	101.98	2950.0	China	Inland (plateau)
12 Xinglong (XL)	40.40	117.58	960.0	China	Mountain (semiarid)

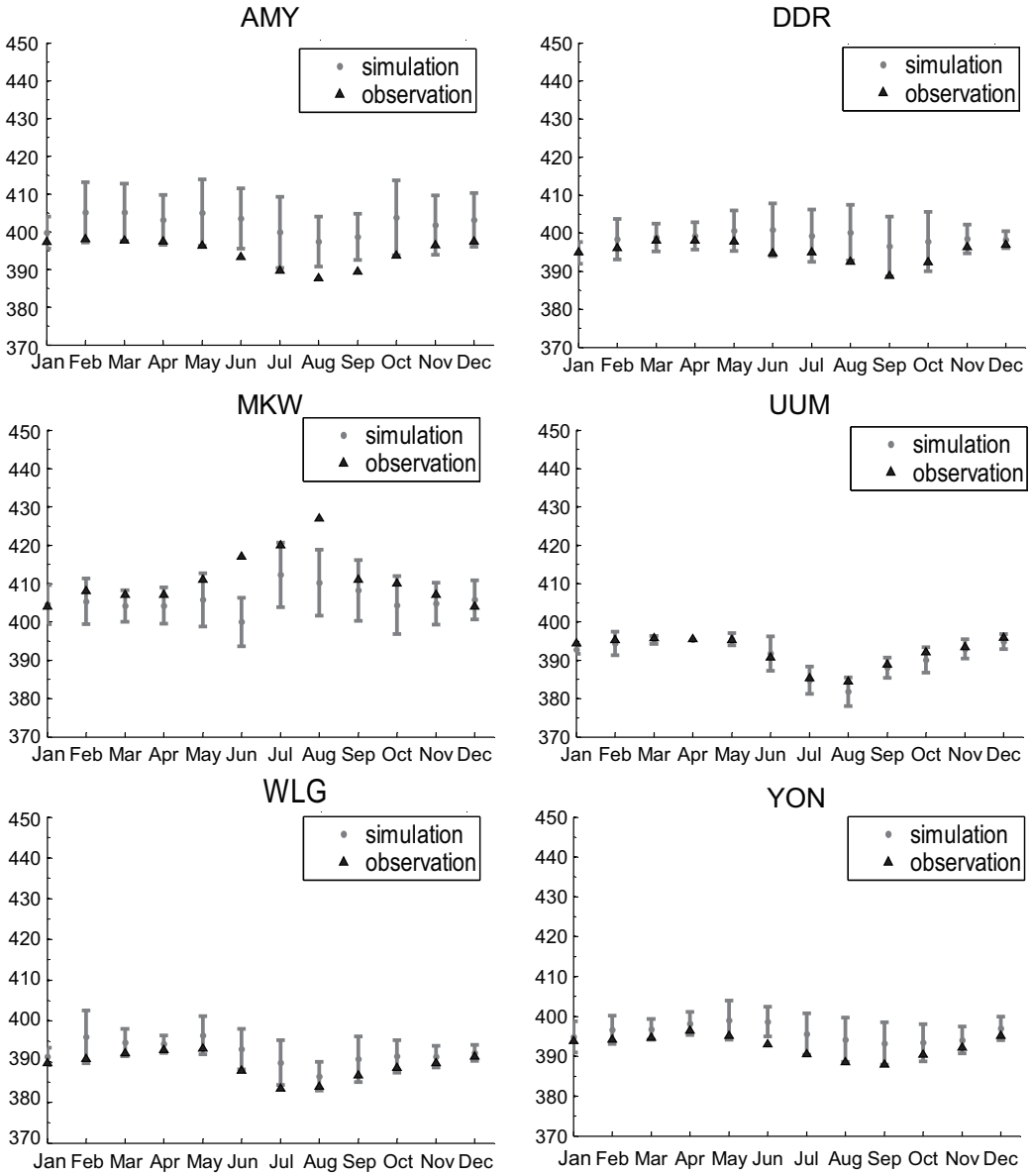

Fig. 5. Monthly-averaged CO_2 concentrations for the simulation (grey) and observation (black) from January to December at stations AMY, DDR, MKW, UUM, WLG and YON, with standard deviation ($\pm$) of the simulation provided (units: ppm).

acteristics are listed in Table 3. As shown in Fig. 5, simulated CO_2 concentrations were generally in good agreement with observed ones. The CO_2 levels in remote sites were similar (especially in winter; $\sim$ 390 ppm) as a result of comparable bioflux and relatively low anthropogenic influence. CO_2 concentrations were lowest during summer at most sites (except for MKW) owing to the strong biospheric absorption. In addition, AMY, with higher CO_2 all year round than WLG, which is geographically at a similar latitude ($\sim$36.5°N), implies a greater influence of large-scale transport of local emissions (Ballav et al., 2012). Generally, CMAQ performed better during winter, spring and autumn than in summer, which is associated with the strength of terrestrial biosphere impacts. This implies stronger effects of uncertainty in bioflux in the regional CO_2 simulation during summertime, since the uncertainty of bioflux estimation has been found to be seasonally dependent, as reflected by a terrestrial model intercomparison (Huntzinger et al., 2013). Possible reasons also include, but are not restricted to, errors in model transport in the boundary layer, the influence of complex local topography and small-scale system effects, and temporal emissions profiles, as well as the lag effect of the biospheric contribution to the atmospheric concentration in regional CTMs due to the long atmospheric lifetime of CO_2.

For these six stations, the correlation coefficient between simulated and observed monthly mean CO_2 concentrations ranged from 0.34 at MKW to a maximum of 0.98 at UUM (Table 3). The mountain station (DDR) and remote ocean station (YON) showed lower seasonal variation. At the mountain site (DDR), we used the 5th-layer ($\sim$ 750 m AGL, to

Table 3. Statistical characteristics of observed and simulated CO_2 concentrations on a monthly basis in 2010 for stations AMY, DDR, MKW, UUM, WLG and YON.

Station	A_o	A_m	σ_o	σ_m	Bias (%)	RMSE	R
1 AMY	394.5	402.18	3.58	2.56	1.95	2.37	0.75
2 DDR	395.12	398.63	2.65	1.63	0.89	2.57	0.35
3 MKW	411.08	404.48	6.64	1.17	−1.61	6.34	0.34
4 UUM	392.21	391.48	3.92	4.30	−0.19	0.95	0.98
5 WLG	390.06	392.28	2.56	2.73	0.57	1.34	0.87
6 YON	392.65	395.98	2.62	1.97	0.85	1.62	0.79

Notes: A_o = average of observation; A_m = average of simulation; σ_o = standard deviation of observation; σ_m = standard deviation of simulation; Bias = (simulation – observation)/observation × 100%; RMSE = root-mean-square error between simulation and observation; R = correlation coefficient between simulation and observation.

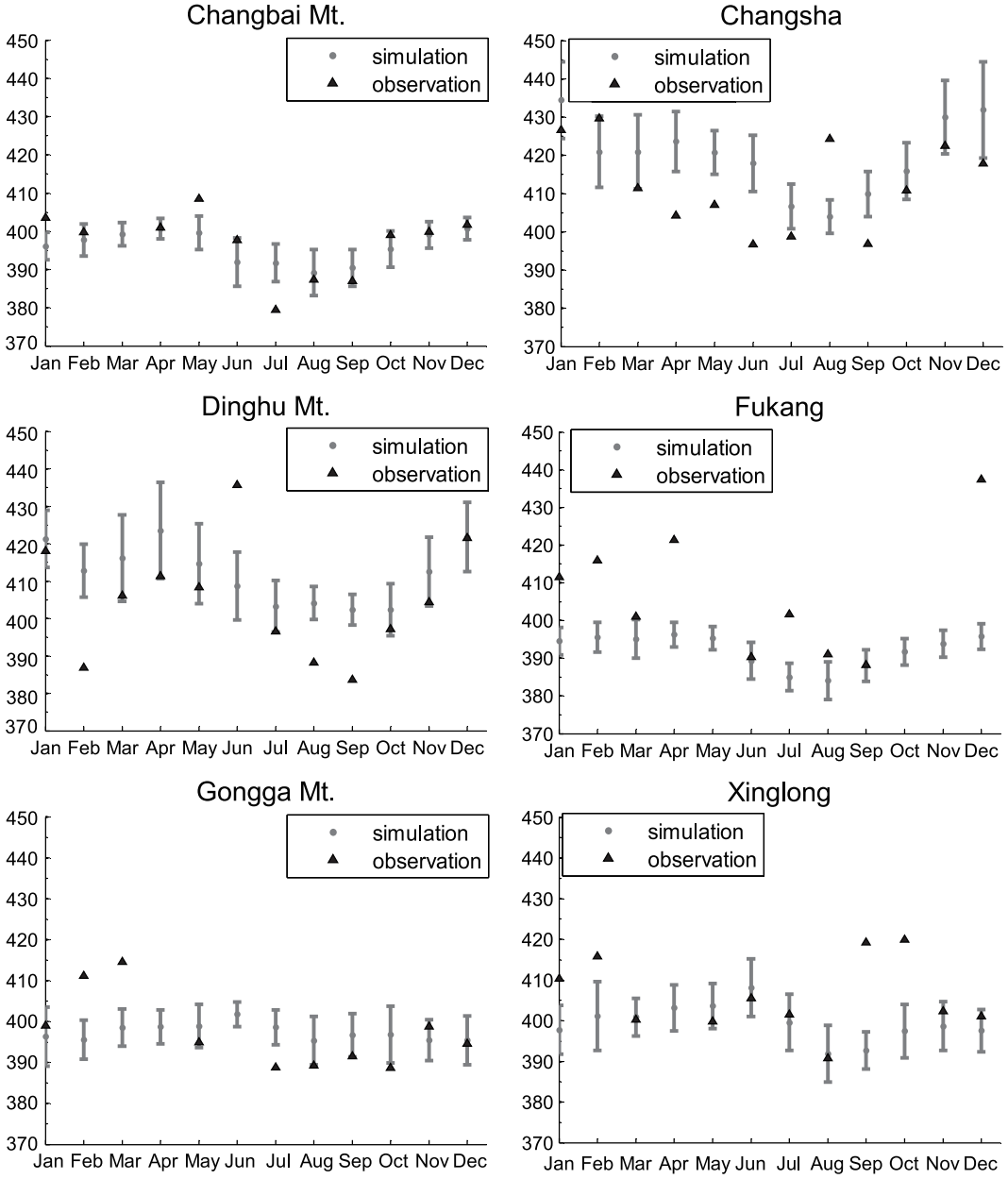

Fig. 6. The same as Fig. 5 but for the stations of Changbai Mountains, Changsha, Dinghu Mountains, Fukang, Gongga Mountains, and Xinglong.

approach the real height) CMAQ results to compare with the observations. The bias between the simulation and observations infers a difficulty for the model to capture the influence of such complex local topography. At the remote stations of WLG and UUM, mostly driven by long-range transport and local biospheric flux, CMAQ reasonably reproduced the monthly variations with mean biases of 0.57% and −0.19%, and correlation coefficients of 0.87 and 0.98, respectively. MKW is unique and of higher interest compared to the other sites, not only because it frequently receives local fossil-fuel emissions from Nagoya, but also because it shows different seasonality of higher CO_2 levels in summer and lower values in the other seasons. As can be seen in Fig. 5, CMAQ demonstrated potential in reproducing the monthly-averaged CO_2 concentrations at urban sites dominated by anthropogenic emissions, but with a lower bias in summer. Bioflux estimation by interpolation of the CT2011_oi results with global resolution of 3° (lon) ×2° (lat) tends to be hard for resolving the urban ecosystem conditions. Also, it was difficult for the model with its 64 km ×64 km horizontal resolution to capture the influence from complex local topography and small-scale system effects. Attributing the underestimation at urban sites during summertime to errors in fossil-fuel emissions, bioflux, or model transport would lead to drastically different conclusions (i.e., upscaling emissions in the first versus no scaling in the latter two) (McKain et al., 2012). Also, it should be noted that not all urban stations exhibit such a seasonal pattern due to variation in anthropogenic emissions and urban ecosystem conditions.

The seasonality of surface CO_2 concentrations at six CERN sites is summarized in Fig. 6. These six sites, spreading from south to north China with different terrestrial ecosystems, cover both fast-developing regions (e.g., Dinghu Mountains in the Pearl River Delta region, Changsha Station in Southeast China, and Xinglong in the Beijing–Tianjin–Hebei city cluster), and non-urban regions (e.g., Changbai Mountains in the forests of the northeast, Fukang Station in the deserts of the northwest, and Gongga Mountains on the Tibetan Plateau). Monthly-mean CO_2 observations at the surface sites exhibited maxima in winter and minima in summer due to variation in bioflux magnitude as well as regional anthropogenic emissions. The summertime trough of CO_2 concentrations was well captured by the model. Figure 6 shows that the CO_2 concentrations of Changbai Mountains, Dinghu Mountains, Xinglong and Fukang exhibited strong seasonal variation, with differences between the maximum and minimum monthly means being as large as ∼ 20 ppm. As for the urban site at Changsha, observed monthly CO_2 concentrations displayed a summertime trough but with a sharp increase in August. Monthly CO_2 at Gongga Mountains showed little seasonal variation due to the cold wet climate throughout the year, which is unfavorable for the growth of plants. In general, the model reproduced the monthly mean mixing ratios of CO_2 as well as the seasonal variations, while major deficiencies included an underestimation of CO_2 at Fukang and Xinglong and an overestimation at Changsha. The discrepancy was probably due to the uncertainty in input fluxes and the model's inability to resolve the complex local topography and small-scale system effects with its 64 km ×64 km resolution (van der Molen and Dolman, 2007; Kou et al., 2013). In addition, the fact that the model results were not sampled for the specific time when the measurements were conducted could explain part of the bias between them and the observations.

Although several biases with the model have been identified based on the results presented in Figs. 5 and 6, we can see that the CO_2 spatial variation in urban and non-urban regions was reproduced well by CMAQ, and the evaluation against observations lends confidence to the model's ability in capturing the general seasonal pattern of surface CO_2 concentration in East Asia. Therefore, we do not expect the model biases to change the main findings of the present study on the regionally and monthly-averaged general seasonality of surface CO_2 over East Asia.

3.2. *Impacts of bioflux on surface CO_2 concentrations*

The horizontal distributions of simulated seasonal mean CO_2 concentrations of the standard simulation in winter, spring, summer and autumn are presented in Figs. 7a–d. As expected, the CMAQ simulation showed an ability to resolve the fine-scale features with numerous hotspots and stronger spatial heterogeneity of CO_2 while in general retaining the large-scale spatial patterns. Discernible gradients in CO_2 could be seen between northwestern and eastern China. CO_2 concentrations above 425 ppm were found over North China, and the Southeast China coastal regions, where intensive human activities are concentrated. This feature was in agreement with the CO_2 net fluxes distribution pattern (Fig. 3). Characterized by a high frequency of steady winds, inverse temperature structure (Ge et al., 2011), and considerable emissions (Fig. 3), higher levels of CO_2 were also found in the Sichuan Basin. Careful analyses of the results suggested that it is not appropriate to generalize one seasonal pattern for surface CO_2 concentrations that fits situations across all parts of East Asia.

Seasonal CO_2 variations were particularly high in East Asia, with higher concentrations in winter, lower concentrations in spring and autumn, and the lowest concentrations in summer. From Fig. 7a it can be seen that the high CO_2 concentrations were mainly distributed over regions with intensive human activities during wintertime. Following the wind pattern controlled by the Siberian High, the surface winds were initially northeastwards in northern China, Japan, and Korea. Thus, higher emissions as well as transport together contributed to the accumulation of CO_2 in these areas. In summer (Fig. 7c), CO_2 concentrations of less than 410 ppm (less than 435 ppm in urban regions) were found in most areas of Southeast China. The CO_2 values in the North China Plain, Korea and eastern Japan were found to be higher than 420 ppm. In addition to the anthropogenic input of fossil fuels combustion and residential emissions, possible reasons also include the monsoon transition process of prevailing south and southeast winds pushing pollution northwards and contributing to the higher CO_2 levels in this area. Overall, Figs.

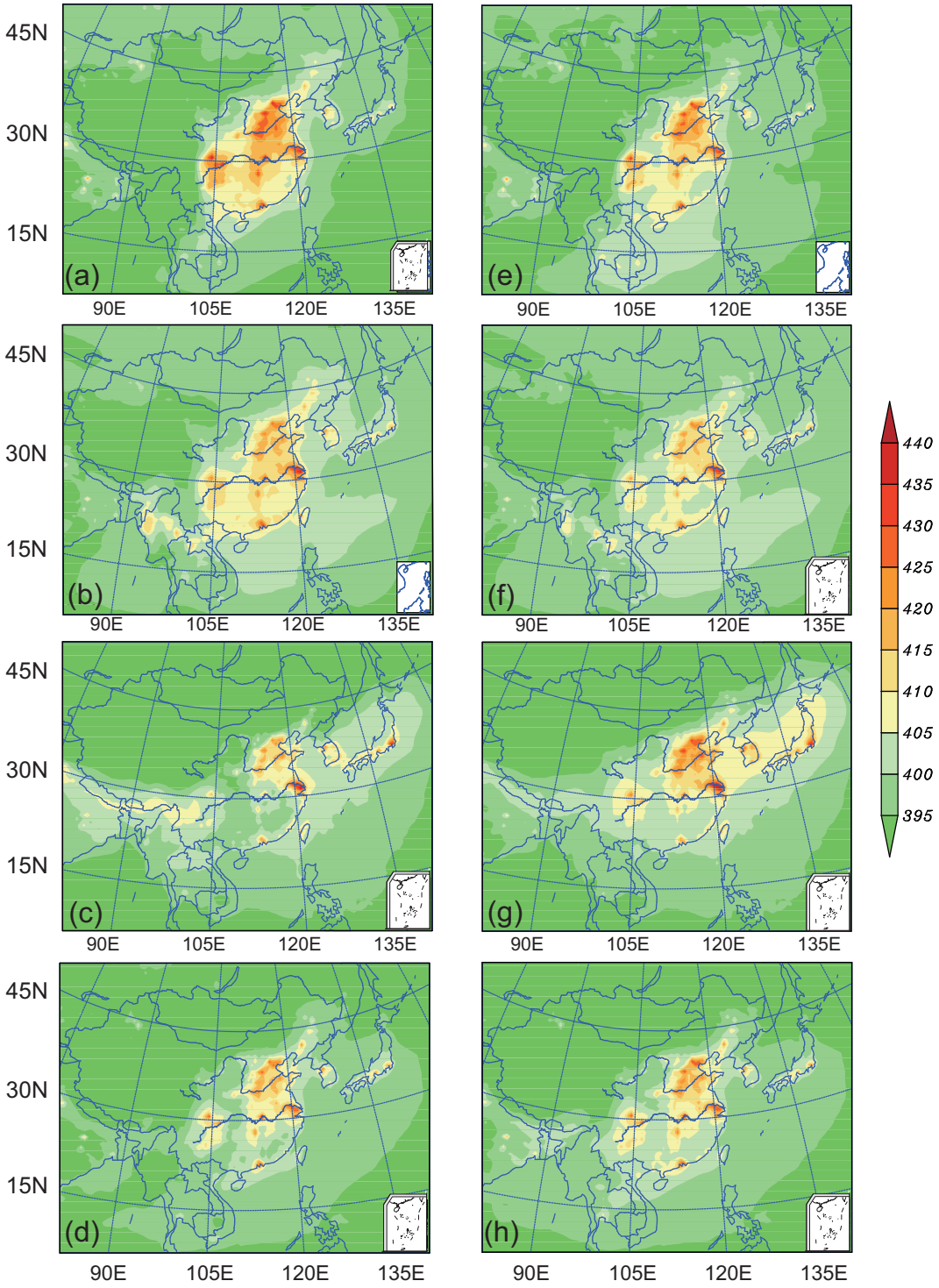

Fig. 7. Horizontal distribution of CO_2 concentrations near the surface from the standard simulation (with prescribed bioflux) in (a) winter, (b) spring, (c) summer, and (d) autumn; and the comparison (without bioflux) simulation in (e) winter, (f) spring, (g) summer, and (h) autumn (units: ppm).

7a–d demonstrate that the much-refined descriptions of transport and emissions in CMAQ allows for a more detailed characterization of the spatial distribution of CO_2 and can facilitate an interpretation of sparse observational data in a regional context over East Asia. Next, we discuss the role of biospheric flux in shaping the spatial patterns of CO_2 by comparing the results from the standard and comparison simulation.

Figures 7e–h show the results of the CMAQ simulation without prescribed biospheric flux, and Fig. 8 provides the

difference between the standard and the comparison simulation. Upon examination of the results of the standard simulation (Figs. 7a–d), those of the comparison simulation (Figs. 7e–h) exhibit a similar spatial pattern throughout the year. For example, the steep gradients in CO_2 between northwestern and eastern China in Figs. 7a–d can still be seen in Figs. 7e–h. Numerous domes of CO_2 ($\geqslant$ 435 ppm) formed near large fossil-fuel emissions sources (as shown in Fig. 2). The dispersion of CO_2 from these domes and from smaller emissions sources resulted in an increase of CO_2 in the surrounding areas.

The bioflux, acting as a net source or sink due to the growth or decay of the terrestrial biosphere during various seasons and regions, is identified as the dominant control for atmospheric CO_2 seasonal variation (as shown in Fig. 8). This is further superimposed on regional patterns of anthropogenic contribution, rather than at scattered spots. Surface CO_2 concentrations in the comparison simulation were much lower than in the standard simulation during winter and spring, and much higher during summer and autumn, in most areas. A weaker CO_2 enhancement and reduction could be seen in the northwest of China due to lower bioflux absolute values (Figs. 2a–d). The decrease of CO_2 concentrations constrained by biospheric fluxes usually occurred in summer and, to a lesser degree, in autumn. Moreover, Fig. 7c shows that summertime CO_2 greater than 415 ppm often appeared over Korea and Japan, North China, and coastal regions of Southeast China; whereas in the comparison results (Fig. 7g), the areas ($>$ 415 ppm) appeared over a much larger scale. The different variation identified here could perhaps be explained by the associated terrestrial biosphere distribution (Figs. 2a–d), suggesting that bioflux offsetting anthropogenic CO_2 emissions would lead to distinctly different surface CO_2 conditions. A comparison of Figs. 7 and 8 suggests that (1) bioflux dominates the distribution pattern in areas far away from large anthropogenic perturbations; and (2) the biospheric contribution in the majority of cities cannot be regarded as negligible according to the specific urban ecosystem conditions.

The sensitivity experiments also facilitated the interpretation of CO_2 distribution and suggested a comparable importance of biospheric fluxes and fossil-fuel emissions in shaping spatial distributions of CO_2 near the surface over the model domain. For example, Figs. 7 and 8 clearly show that anthropogenic inputs and transport processes were the major contributors in forming the hotspots of CO_2 concentration in the east of Japan (as for the situation of MKW, discussed above) during summer (Fig. 7g), while biospheric fluxes helped offset the high concentration in this area by $\sim$ 3–7 ppm (Fig. 8c). Moreover, the terrestrial biosphere brought about great reduction in surface CO_2 concentrations ($\geqslant$ 7 ppm) during summer in most areas of the model domain, except for the Indo-China Peninsula where positive bioflux was found during this period (Fig. 2c). As can be seen in Fig. 8a, the biosphere played an important role in elevating the CO_2 levels in most areas during winter ($\geqslant$ 3 ppm

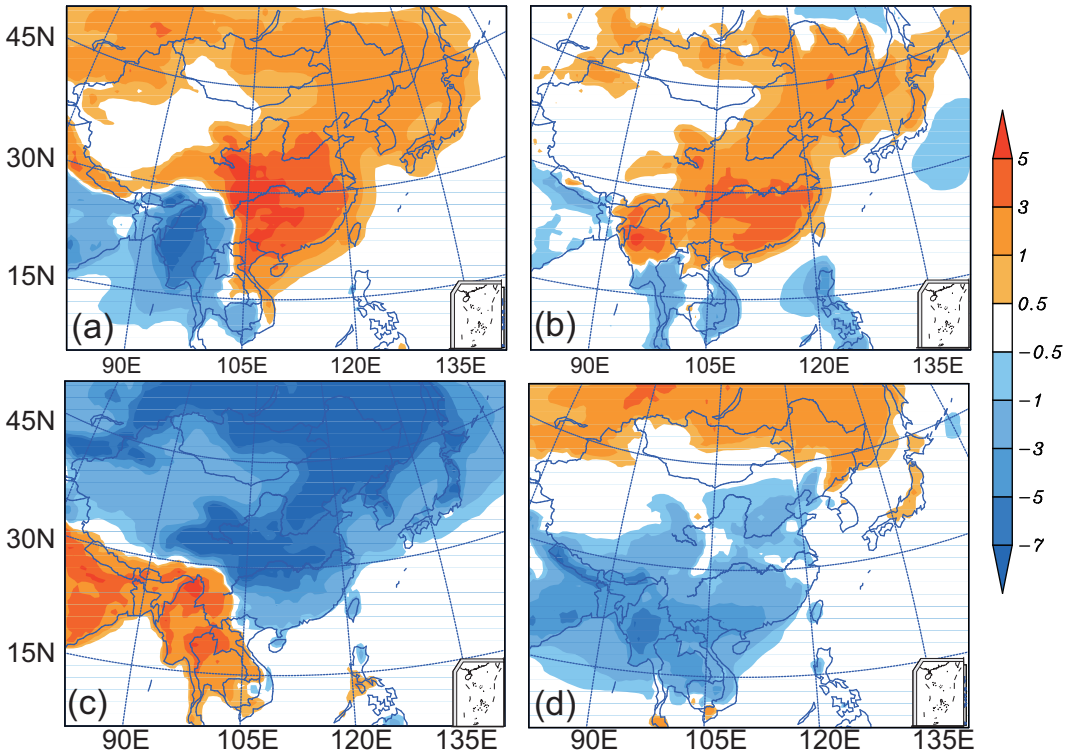

Fig. 8. The difference in horizontal distribution of CO_2 concentrations between the two sets of simulations (i.e., the results of that without prescribed bioflux subtracted from the results of that with bioflux): (a) winter, (b) spring, (c) summer, and (d) autumn (units: ppm).

in North China and Southeast China, and $\geqslant 5$ ppm in the Sichuan Basin), although the anthropogenic inputs and meteorological conditions had already caused an accumulation of CO_2 in these areas (Fig. 7a). In addition, it is interesting that the areas with decreased CO_2 concentration in autumn (Fig. 8d) were much larger than the negative bioflux areas shown in Fig. 2d. Such regionally varied situations imply that for conclusions to be drawn regarding carbon sinks and sources, functional areas of terrestrial ecosystems and the associated transport mechanisms both need to be further examined when investigating the contribution of the biosphere (i.e., magnify or shrink the atmospheric CO_2 levels).

4. Summary and conclusions

In this study, seasonal variations of surface CO_2 concentrations in East Asia were investigated by applying a comprehensive regional air quality modeling system, RAMS-CMAQ, with prescribed CO_2 fluxes that included fossil-fuel emissions, biomass burning, ocean flux, and biosphere–atmosphere exchange. The biospheric contribution to regulating the spatiotemporal distribution and seasonal patterns of CO_2 near the surface over East Asia was assessed. The results demonstrated the potential of regional CTMs (CMAQ, in this case) to facilitate interpretations of CO_2 observations, and resolve fine-scale features. The comparison of the model results with ground-based in-situ measurements indicated that the model reproduces temporal and spatial variations of CO_2 concentrations reasonably well, but with a higher bias during the growing season (especially summer), implying stronger effects of uncertainty in bioflux estimation in regional simulations during summertime. Careful analyses of the results suggested that it is not appropriate to generalize one seasonal pattern for surface CO_2 concentrations to fit situations across all parts of East Asia.

The results of the sensitivity experiments showed that biospheric fluxes and fossil-fuel emissions are comparably important in shaping spatial distributions of surface CO_2 concentrations over East Asia. Fossil-fuel emissions play an important role in shaping the general spatial distribution of CO_2 near the surface over East Asia, whereas biospheric flux is responsible for the prevailing spatial pattern of CO_2 enhancement and reduction on the synoptic scale. The contribution of the biospheric CO_2 component varies significantly due to the strong seasonality of biospheric flux. In winter, the increases of CO_2 levels by the biosphere were found to be larger than 5 ppm in North China and Southeast China, and during summertime the biosphere made a great reduction ($\geqslant 7$ ppm) in most areas, except for the Indo-China Peninsula where positive bioflux was found. In areas far away from large anthropogenic perturbations, the biospheric contribution dominates the spatial pattern of surface CO_2 distribution; while in densely urbanized regions the biospheric contribution cannot be regarded as negligible due to the specific urban ecosystem conditions. The results presented here also serve as a foundation for future work in which further comprehensive examinations of CO_2 spatiotemporal variability and the various associated uncertainties are performed.

Acknowledgements. This work was supported by the Strategic Priority Research Program–Climate Change: Carbon Budget and Relevant Issues (Grant No. XDA05040404), the National High Technology Research and Development Program of China (Grant No. 2013AA122002), and the National Natural Science Foundation of China (Grant No. 41130528). This study used ground-based in-situ CO_2 concentration observations from the stations of AMY, DDR, MKW, UUM, WLG, YON (WDCGG), Changbai Mt., Changsha, Dinghu Mt., Fukang, Gongga Mt., and Xinglong (CERN). We express deep gratitude to the dedicated principal investigators, research teams and support staff of the stations for providing their CO_2 observation records on the WDCGG website. Also, we would like to express deep appreciation to SCAS-CERN for providing CO_2 measurements. CarbonTracker results used in the model as initial fields, boundary conditions and bioflux estimations were provided by NOAA ESRL, Boulder, Colorado, USA, http://carbontracker.noaa.gov.

REFERENCES

Ahmadov, R., C. Gerbig, R. Kretschmer, S. Koerner, B. Neininger, A. J. Dolman, and C. Sarrat, 2007: Mesoscale covariance of transport and CO_2 fluxes: Evidence from observations and simulations using the WRF-VPRM coupled atmosphere-biosphere model. *J. Geophys. Res.*, **112**, D22, doi: 10.1029/2007jd008552.

Ahmadov, R., C. Gerbig, R. Kretschmer, S. Körner, C. Rödenbeck, P. Bousquet, and M. Ramonet, 2009: Comparing high resolution WRF-VPRM simulations and two global CO_2 transport models with coastal tower measurements of CO_2. *Biogeosciences*, **6**, 807–817, doi: 10.5194/bg-6-807-2009.

Ballav, S., and Coauthors, 2012: Simulation of CO_2 concentration over East Asia using the regional transport model WRF-CO_2. *J. Meteor. Soc. Japan*, **90**(6), 959–976, doi: 10.2151/jmsj.2012-607.

Canadell, J. G., and Coauthors, 2007: Contributions to accelerating atmospheric CO_2 growth from economic activity, carbon intensity, and efficiency of natural sinks. *Proc. Natl. Acad. Sci. USA*, **104**, 18866–18870, doi: 10.1073/pnas.0702737104.

Chevillard, A., U. Karstens, P. Ciais, S. Lafont, and M. Heimann, 2002: Simulation of atmospheric CO_2 over Europe and western Siberia using the regional scale model REMO. *Tellus (B)*, **54**, 872–894, doi: 10.1034/j.1600-0889.2002.01340.x.

Conway, T. J., 2013: Atmospheric CO_2 monthly concentration data, Ulaan Uul, World Data Centre for Greenhouse Gases, Japan Meteorology Agency, Tokyo. [Available online at http://ds.data.jma.go.jp/gmd/wdcgg/.]

Fu, Y., and Coauthors, 2009: Environmental influences on carbon dioxide fluxes over three grassland ecosystems in China. *Biogeosciences*, **6**, 2879–2893, doi: 10.5194/bg-6-2879-2009.

Fukuyama, Y., 2013: Atmospheric CO_2 monthly concentration data, Yonagunijima, World Data Centre for Greenhouse Gases, Japan Meteorology Agency, Tokyo. [Available online at http://ds.data.jma.go.jp/gmd/wdcgg/.]

Ge, C., M. G. Zhang, L. Y. Zhu, X. Han, and J. Wang, 2011: Simulated seasonal variations in wet acid depositions over

East Asia. *J. Air Waste Manage. Assoc.*, **61**, 1246–1261, doi: 10.1080/10473289.2011.596741.

Gurney, K. R., Y. H. Chen, T. Maki, S. Randy Kawa, A. Andrews, and Z. X. Zhu, 2005: Sensitivity of atmospheric CO_2 inversions to seasonal and interannual variations in fossil fuel emissions. *J. Geophys. Re*s., **110**, D10308, doi: 10.1029/2004JD005373.

Huntzinger, D. N., and Coauthors, 2012: North American Carbon Program (NACP) regional interim synthesis: Terrestrial biospheric model intercomparison. *Ecol. Model.*, **232**, 144–157, doi: 10.1016/j.ecolmodel.2012.02.004.

Huntzinger, D. N., and Coauthors, 2013: The North American carbon program Multi-scale synthesis and terrestrial model intercomparison project-part 1: Overview and experimental design. *Geosci. Model Dev. Discuss.*, **6**, 3977–4008, doi: 10.5194/gmdd-6-3977-2013.

Kou, X. X., M. G. Zhang, and Z. Peng, 2013: Numerical simulation of CO_2 concentrations in East Asia with RAMS-CMAQ. *Atmos. Oceanic Sci. Lett.*, **6**(4), 179–184, doi: 10.3878/j.issn.1674-2834.13.0022.

Kurokawa, J., and Coauthors, 2013: Emissions of air pollutants and greenhouse gases over Asian regions during 2000–2008: Regional Emission inventory in Asia (REAS) version 2. *Atmos. Chem. Phys.*, **13**, 11019–11058, doi: 10.5194/acp-13-11019-2013.

Le Quere, C., and Coauthors, 2009: Trends in the sources and sinks of carbon dioxide. *Nat. Geosci.*, **2**, 831–836, doi: 10.1038/ngeo689.

Lee, H., and S. H. Kim, 2013: Atmospheric CO_2 monthly concentration data, Anmyeon-do, World Data Centre for Greenhouse Gases, Japan Meteorology Agency, Tokyo. [Available online at http://ds.data.jma.go.jp/gmd/wdcgg/.]

Leung, L. R., S. J. Ghan, Z. C. Zhao, Y. Luo, W. C. Wang, and H. L. Wei, 1999: Intercomparison of regional climate simulations of 1991 summer monsoon in Eastern Asia. *J. Geophys. Res.*, **104**, 6425–6454, doi: 10.1029/1998JD200016.

Liu, J. Y., H. Q. Tian, M. L. Liu, D. F. Zhuang, J. M. Melillo, and Z. X. Zhang, 2005: China's changing landscape during the 1990s: Large-scale land transformations estimated with satellite data. *Geophys. Res. Lett.*, **32**, L02405, doi: 10.1029/2004GL021649.

Liu, M. M., and Coauthors, 2013a: Refined estimate of China's CO_2 emissions in spatiotemporal distributions. *Atmos. Chem. Phys. Discuss.*, **13**, 17 451–17 478, doi: 10.519/acpd-13-17451-2013.

Liu Z., and Coauthors, 2013b: Toward verifying fossil fuel CO_2 emissions with the Community Multi-scale Air Quality (CMAQ) model: Motivation, model description and initial simulation. *J. Air Waste Manage. Assoc.*, **64**, 419–435. doi: 10.1080/10962247.2013.816642.

Lü, A. F., H. Q. Tian, M. L. Liu, J. Y. Liu, and J. M. Melillo, 2006: Spatial and temporal patterns of carbon emissions from forest fires in China from 1950 to 2000. *J. Geophys. Res.*, **111**, doi: 10.1029/2005JD006198.

McKain, K., S. C. Wofsy, T. Nehrkorn, J. Eluszkiewicz, J. R. Ehleringer, and B. B. Stephens, 2012: Assessment of ground-based atmospheric observations for verification of greenhouse gas emissions from an urban region. *Proc. Natl. Acad. Sci. USA*, **109**, 8423–8428, doi: 10.1073/pnas.1116645109.

Morimoto, S., T. Nakazawa, K. Higuchi, and S. Aoki, 2000: Latitudinal distribution of atmospheric CO_2 sources and sinks inferred by δ^{13}C measurements from 1985 to 1991. *J. Geophys. Res.*, **105**, 24 315–24 326, doi: 10.1029/2000JD900386.

Muto, Y., 2013: Atmospheric CO_2 monthly concentration data, Mt. Dodaira, World Data Centre for Greenhouse Gases, Japan Meteorology Agency, Tokyo. [Available online at http://ds.data.jma.go.jp/gmd/wdcgg/.]

Ohno, K., 2011: Atmospheric CO_2 monthly concentration data, Mikawa-Ichinomiya, World Data Centre for Greenhouse Gases, Japan Meteorology Agency, Tokyo. [Available online at http://ds.data.jma.go.jp/gmd/wdcgg/.]

Peters, W., and Coauthors, 2007: An atmospheric perspective on North American carbon dioxide exchange: CarbonTracker. *Proc. Natl. Acad. Sci. USA*, **104**, 18 925–18 930, doi: 10.1073/pnas.0708986104.

Peters, W., and Coauthors, 2010: Seven years of recent European net terrestrial carbon dioxide exchange constrained by atmospheric observation. *Glob. Change Biol.*, **16**, 1317–1337, doi: 10.1111/j.1365-2486.2009.02078.x.

Piao, S., P. Friedlingstein, P. Ciais, N. Viovy, and J. Demarty, 2007: Growing season extension and its impact on terrestrial carbon cycle in the Northern Hemisphere over the past decades. *Global Biogeochemical Cycles*, **21**, GB3018, doi: 10.1029/2006GB002888.

Piao, S., J. Fang, P. Ciais, P. Peylin, Y. Huang, S. Sitch, and T. Wang., 2009: The carbon balance of terrestrial ecosystems in China. *Nature*, **458**, 1009–1013, doi: 10.1038:/nature07944.

Sarrat, C., and Coauthors, 2007: Atmospheric CO_2 modeling at the regional scale: Application to the CarboEurope Regional Experiment. *J. Geophys. Res.*, **112**, D12, doi: 10.1029/2006jd008107.

Schaefer, K., and Coauthors, 2012: A model-data comparison of gross primary productivity: Results from the North American Carbon Program site synthesis. *J. Geophys. Res.*, **117**, G03010, doi: 10.1029/2012jg001960.

Schneising, O., J. Heymann, M. Buchwitz, M. Reuter, H. Bovensmann, and J. P. Burrows, 2013: Anthropogenic carbon dioxide source areas observed from space: Assessment of regional enhancements and trends. *Atmos. Chem. Phys.*, **13**, 2445–2454, doi: 10.5194/acp-13-2445-2013.

Solomon, S., and Coauthors, 2007: *Climate Change 2007: The Physical Science Basis, Contribution of Working Group I to the Fourth Assessment Report of the Intergovernmental Panel on Climate Change*, Cambridge Univ. Press, 996 pp.

Streets, D. G., and Coauthors, 2003a: An inventory of gaseous and primary aerosol emissions in Asia in the year 2000. *J. Geophys. Res.*, **108**(D21), 8809, doi: 10.1029/2002JD003093.

Streets, D. G., K. F. Yarber, J. H. Woo, and G. R. Carmichael, 2003b: Biomass burning in Asia: Annual and seasonal estimates and atmospheric emissions. *Global Biogeochemical Cycles*, **17**(4), 1099, doi: 10.1029/2003GB002040.

van der Molen, M. K., and A. J. Dolman, 2007: Regional carbon fluxes and the effect of topography on the variability of atmospheric CO_2. *J. Geophys. Res.*, **112**(D1), doi: 10.1029/2006jd007649.

van der Werf, G. R., and Coauthors, 2010: Global fire emissions and the contribution of deforestation, savanna, forest, agricultural, and peat fires (1997–2009). *Atmos. Chem. Phys.*, **10**, 11 707–11 735, doi: 10.5194/acp-10-11707-2010.

Wang, H., R. Zhang, M. Liu, and J. Bi, 2012: The carbon emissions of Chinese cities. *Atmos. Chem. Phys.*, **12**, 6197–6206, doi: 10.5194/acp-12-6197-2012.

Wang, J., Q. Bao, N. Zeng, Y. M. Liu, G. X. Wu, and D. Y. Ji, 2013: Earth system model FGOALS-s2: Coupling a dynamic global

vegetation and terrestrial carbon model with the physical climate system model. *Adv. Atmos. Sci.*, **30**(6), 1549–1559, doi: 10.1007/s00376-013-2169-1.

Xu, Y. F., Y. C. Li, and M. Chu, 2013: A global ocean biogeochemistry general circulation model and its simulations. *Adv. Atmos. Sci.*, **30**(3), 922–939, doi: 10.1007/s00376-012-2162-0.

Yu, G. R., and Coauthors, 2013: Spatial patterns and climate drivers of carbon fluxes in terrestrial ecosystems of China. *Global Change Biology*, **19**, 798–810, doi: 10.1111/gcb.12079.

Zhang, M. G., I. Uno, S. Sugata, Z. F. Wang, D. Byun, and H. Akimoto, 2002: Numerical study of boundary layer ozone transport and photochemical production in East Asia in the wintertime. *Geophys. Res. Lett.*, **29**(11), 40-1–40-4, doi: 10.1029/20001GL014368.

Zhang, Q., and Coauthors, 2009: Asian emission in 2006 for the NASA INTEX-B mission. *Atmos. Chem. Phys.*, **9**, 5131–5153, doi: 10.5194/acp-9-5131-2009.

Zhang, Y., J. Zhang, and C. P. Nielsen, 2013: The effects of recent control policies on trends in emissions of anthropogenic atmospheric pollutants and CO_2 in China. *Atmos. Chem. Phys.*, **13**, 487–508, doi: 10.5194/acp-13-487-2013.

Zhao, Y., C. P. Nielsen, and M. B. McElroy, 2012: China's CO_2 emissions estimated from the bottom up: Recent trends, spatial distributions, and quantification of uncertainties. *Atmos. Environ.*, **59**, 214–223, doi: 10.1016/j.atmosenv.2012.05.027.

Zhou, L. X., 2013: Atmospheric CO_2 monthly concentration data, Mt. Waliguan, World Data Centre for Greenhouse Gases, Japan Meteorology Agency, Tokyo. [Available online at http://ds.data.jma.go.jp/gmd/wdcgg/.]